High-frequency operation of a mid-infrared interband cascade system at room temperature

Hossein Lotfi,[1,a)] Lu Li,[1] Lin Lei,[1,2] Hao Ye,[1] S. M. Shazzad Rassel,[1] Yuchao Jiang,[1] Rui Q. Yang,[1,b)] Tetsuya D. Mishima,[2] Michael B. Santos,[2] James A. Gupta,[3] and Matthew B. Johnson[2]

[1]*School of Electrical and Computer Engineering, University of Oklahoma, Norman, Oklahoma 73019, USA*
[2]*Homer L. Dodge Department of Physics and Astronomy, University of Oklahoma, Norman, Oklahoma 73019, USA*
[3]*National Research Council of Canada, Ottawa K1A 0R6, Canada*

(Received 16 March 2016; accepted 3 May 2016; published online 16 May 2016)

The high-frequency operation of a mid-infrared interband cascade system that consists of a type-I interband cascade laser and an uncooled interband cascade infrared photodetector (ICIP) is demonstrated at room temperature. The 3-dB bandwidth of this system under direct frequency modulation was ~850 MHz. A circuit model was developed to analyze the high-frequency characteristics. The extracted 3-dB bandwidth for an uncooled ICIP was ~1.3 GHz, signifying the great potential of interband cascade structures for high-speed applications. The normalized Johnson-noise-limited detectivity of these ICIPs exceeded 10^9 cm $Hz^{1/2}$/W at 300 K. These results validate the advantage of ICIPs to achieve both high speed and high sensitivity at high temperatures. *Published by AIP Publishing.*
[http://dx.doi.org/10.1063/1.4950700]

Interband cascade (IC) lasers (ICLs)[1] can be combined with interband cascade infrared photodetectors (ICIPs)[2] or interband cascade photovoltaic devices (ICPVs)[3] to build a functional interband cascade system with devices either on closely packaged units or on a single chip. The system will be compact and portable, because IC devices can be operated efficiently with high performance characteristics and low power consumption[4] (e.g., low threshold current density for ICLs and high detectivity for ICIPs) at room temperature and above. These features are important for many applications such as chemical sensing, free space optical communication, and power beaming. Additionally, some specific applications, such as heterodyne detection and high-bandwidth free-space optical communication, require devices capable of high-frequency operation. Generally, semiconductor lasers are able to operate at high frequencies (with bandwidths in the GHz range) with appropriate packaging, as was verified for ICLs at low temperatures with operation up to 3.2 GHz.[5,6] However, it is difficult for conventional photodetectors to achieve high-frequency operation without sacrificing sensitivity. This difficulty can be significantly alleviated or circumvented in ICIPs, whose high-frequency characteristics are the main focus of this letter.

The 3-dB bandwidth for a conventional photodetector with a single absorber, in which the diffusion process controls the carrier transport, is $f_{3\text{-}dB} = \frac{2.43D}{2\pi t^2}$,[7] where D and t are the diffusion coefficient and the absorber thickness, respectively. Therefore, the device bandwidth will be increased by reducing the absorber thickness. However, this would also reduce the optical absorption and thus the device sensitivity (signal to noise ratio). This compromise can be avoided in ICIPs with a multiple-stage discrete absorber architecture. Each stage is composed of three regions: electron barrier, hole barrier, and the absorber layer, where electron–hole pairs are created by absorbed photons. Each individual absorber is sandwiched between an electron barrier and a hole barrier. As shown in Fig. 1, the photogenerated carriers recombine at the interface between the electron and hole barriers of adjacent cascade stages. Hence, photogenerated carriers travel only a short distance, at most one cascade stage, before being collected at the interfaces of adjacent stages or the contacts. Consequently, when individual absorbers are designed to be short, ICIPs can respond quickly to direct optical modulation at high frequencies while significant absorption of incident light is ensured by multiple absorbers located in each serially connected stage. As such, the total absorber thickness is sufficient to maintain a high absorption efficiency and thus a high sensitivity.[8,9] Therefore, ICIPs have the flexibility to circumvent the limitation on individual absorber thickness due to a finite diffusion length or short transit time requirement, and can achieve high device performance at high temperatures with high-frequency operation. The advantages of a high temperature operation with large device resistance and detectivity and a short response time (on the order of ns) have been demonstrated in previous works,[10–15] but high-frequency operation of ICIPs has not been explored until this work. It is worth noting that intersubband based detectors have been previously studied for high-speed mid-IR detection. However, these intersubband photodetectors require gratings for normal incidence detection, usually work only at low temperatures and have a low photo-response (and a low detectivity) that decreases further at high temperatures.[16–18] These issues in intersubband photodetectors are circumvented in an appropriately designed ICIP.

The ICIP used in this work for studying the high-frequency response was designed with three cascade stages. The individual absorber thickness in every stage was kept short to reduce the carrier transit time across a single stage.

[a)]E-mail: hossein.lotfi@ou.edu
[b)]E-mail: Rui.q.Yang@ou.edu

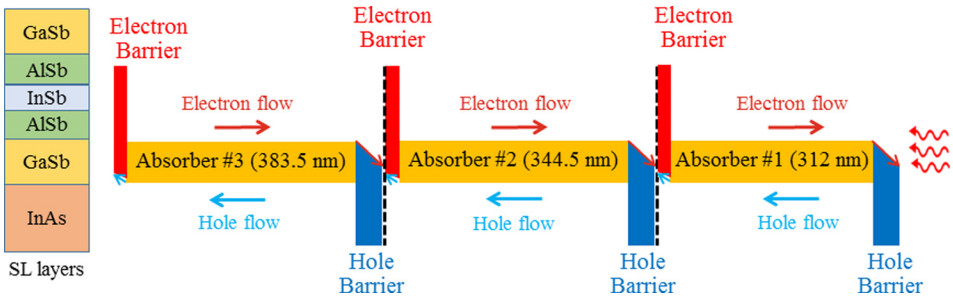

FIG. 1. Schematic diagram of the three-stage ICIP. From right to left, the absorber thicknesses are 312.0, 344.5, and 383.5 nm. The left block is a schematic layer diagram for one period of a SL absorber.

From the surface to the substrate, the absorber thicknesses were 312.0, 344.5, and 383.5 nm. Absorbers were thicker in optically deeper stages to achieve photo-current matching between different stages. Each absorber was composed of a type-II superlattice (SL), in which each period consisted of InAs (27 Å)/GaSb (15 Å)/AlSb (2.7 Å)/InSb (2.6 Å)/AlSb (2.7 Å)/GaSb (15 Å) layers. Similar to previously reported ICIPs,[8,10] electron and hole barriers were made of digitally graded GaSb/AlSb quantum wells (QWs) and InAs/AlSb QWs, respectively. The schematic diagram of this ICIP is shown in Fig. 1. The structure was grown by molecular beam epitaxy (MBE) on a nominally undoped GaSb substrate. After growth, square-mesa ICIPs with side lengths from 20 to 400 μm were defined using conventional contact ultraviolet photolithography and wet etching. For passivation, 174-nm of Si_3N_4 and 224-nm of SiO_2 were deposited by RF sputtering to improve overall stress management and minimize pin holes compared to single-layer passivation. Ti/Au top and bottom contacts were also sputtered. The top metallic contact of all ICIP devices had finger patterns and the devices were illuminated from the top. Finally, the devices were wire bonded for characterization.

The regular spectral response for a representative $200 \times 200\ \mu m^2$ ICIP at 300 K was measured under a zero bias using an FTIR spectrometer and a calibrated 800 K blackbody source. As shown in Fig. 2, the cutoff wavelength was 4.2 μm, corresponding to a bandgap of 0.295 eV and the device responsivity exceeded 0.2 A/W in a broad spectral range. The Johnson-noise-limited detectivity was calculated using $D^* = R_\lambda \sqrt{\frac{R_0 A}{4k_B T}}$, where R_λ, k_B, T, and R_0A are the device responsivity, Boltzmann's constant, the absolute temperature, and the device zero-bias resistance and area product, respectively. D^* quickly reached a value higher than 1.0×10^9 cm Hz$^{1/2}$/W soon after the photon energy exceeded the device bandgap. These values are more than an order of magnitude higher than what was reported for intersubband photodetectors,[18–20] suggesting the suitability of ICIPs for high device performance at room temperature. In the study of high-frequency characteristics, ICIPs with different sizes were used. Values for the zero-bias resistance and area product (R_0A) were extracted from current density (J) and voltage characteristics (e.g., see inset of Fig. 2). For ICIPs made from the same wafer, the average value of R_0A was 0.27 Ω cm^2 and a typical $20 \times 20\ \mu m^2$ ICIP had a resistance of ~35 kΩ at 300 K.

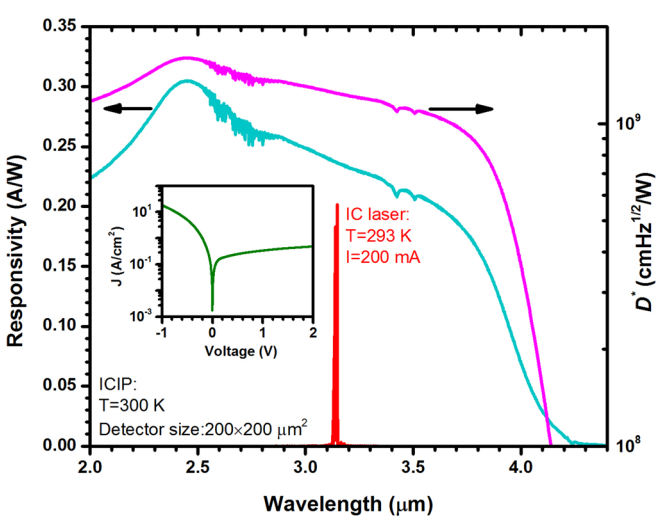

FIG. 2. Zero-bias responsivity and normalized Johnson-noise-limited detectivity for a $200 \times 200\ \mu m^2$ ICIP at 300 K. The IC laser emission spectrum at $T = 293$ K, under 200 mA injection, is also displayed. Inset: dark J–V curve for the same ICIP at 300 K.

A schematic diagram of the interband cascade system for high-frequency modulation is shown in Fig. 3. A narrow ridge type-I ICL[21] (ridge width: 20 μm, cavity length: 2 mm) was used as the mid-IR light source for high frequency modulation measurements. The laser temperature was maintained at $T = 293$ K using a thermoelectric (TE) cooler. The emission wavelength was near 3.15 μm as shown in Fig. 2, with a threshold current density of 405 A/cm^2 at $T = 293$ K. At DC current of 200 mA, the output power was 1.7 mW per facet. A constant-amplitude RF signal with frequency up to 1.2 GHz was sweep generated (with a 2 ms dwell time) by an analog signal generator and was applied to the IC laser using a bias-tee. The laser output beam was then collimated and focused on an uncooled ICIP. A second bias-tee was used to separate the DC and RF signals from the ICIP. The ICIP's RF output was then fed to a spectrum analyzer, and the system frequency spectrum was collected at room temperature. At the laser's emission wavelength, the ICIP's responsivity was 0.24 A/W with a normalized detectivity of 1.2×10^9 cm Hz$^{1/2}$/W. Because of these large values for photo-response and D^*, no RF amplifier was required before the spectrum analyzer. Using the same IC laser, the RF response of the interband cascade system was investigated for ICIPs of different size.

The obtained frequency response of this system with an uncooled $20 \times 20\ \mu m^2$ ICIP at zero-bias is shown in Fig. 4 (top panel). The frequency dependent attenuations of bias-tees and coaxial cables were excluded from the measurements. For this ICIP, the measured 3-dB bandwidth of the system was ~850 MHz at room temperature. Because the IC laser frequency response was not independently measured, the obtained spectra include the frequency response from both the IC laser and the ICIP. To extract their individual frequency responses, an equivalent circuit model was constructed as

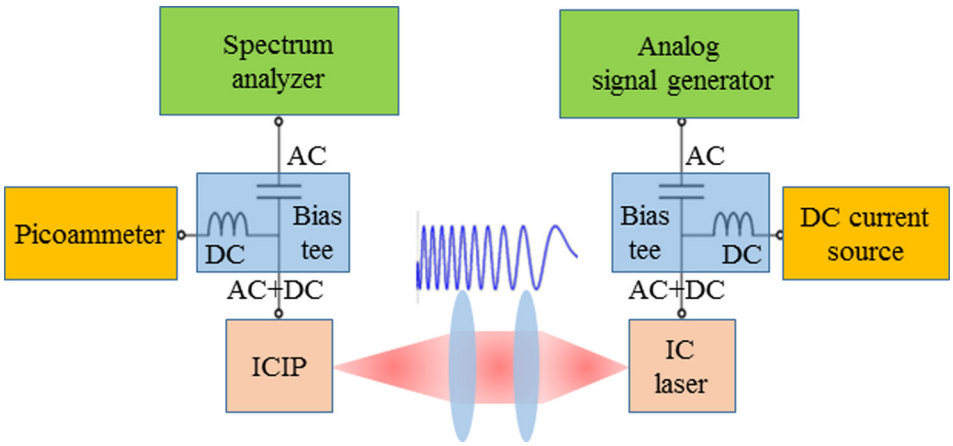

FIG. 3. Schematic drawing of the high frequency mid-IR interband cascade system.

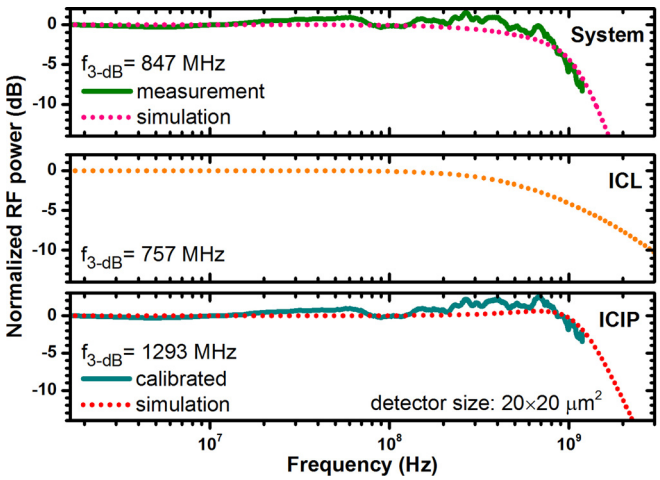

FIG. 4. Measured and simulated frequency response of the interband cascade system with a $20 \times 20\,\mu m^2$ ICIP (top). The calculated frequency response of the type-I IC laser (middle) and the calibrated and simulated frequency response for the ICIP (bottom).

shown in Fig. 5. All the circuit parameters for the IC laser were directly measured and are summarized in Table I; thus its frequency response was independently simulated. The calculated frequency response (R_{ICL}) for the IC laser is shown in Fig. 4 (middle panel). The 3-dB bandwidth of this IC laser was ~760 MHz at $T = 293$ K and was mainly limited by the bonding pad capacitance ($C_{bp} \approx 77.4$ pF). From the R_{ICL} spectrum, the calibrated frequency response of the ICIP(s) can be extracted using $R_{ICIP} = \frac{R_{system}}{R_{ICL}}$, where R_{system} denotes the obtained system frequency response. The extracted frequency response for a $20 \times 20\,\mu m^2$ ICIP is presented in Fig. 4 (bottom panel), which indicates a 3-dB bandwidth of ~1.3 GHz and corresponds to a sub nanosecond response time for this device. At room temperature, the ICIP's resistance R_d was large enough (in the kΩ range and in parallel to an equivalent current source) that it would not affect the modulation bandwidth, which could be considered to be infinite in the response simulations. Similar to the IC laser except for the device capacitance (C_d), all other parameters for the ICIP in the high frequency circuit were directly measured. The series resistance (R_s) was estimated from the measured *I–V* curves at a large forward bias (5 V). The bonding pad capacitance (C_{bp}) related to the two-layer passivation was 1.1 pF for the ICIP. The other high-frequency parasitic element was the parasitic inductance from the gold bonding wires. Depending on the value of parasitic capacitances, at some frequencies, this inductance can counterbalance the capacitive behavior of the circuit, but will cause a sharp decrease in the RF signal at higher frequencies. The ICIP's capacitance (C_d), as the only unknown parameter, was set as a fitting parameter. A curve based on the fitted capacitance is also shown in the top and bottom panels in Fig. 4. The measured and extracted parameters are listed in Table II for two different ICIPs with $20 \times 20\,\mu m^2$ and $30 \times 30\,\mu m^2$ mesa sizes. The observed size dependence of the bandwidth suggests that the 3-dB bandwidth was not limited by the fundamental carrier transit time. This implies that the bandwidth of this interband cascade system can be increased further by reducing the parasitic capacitances and inductances, along

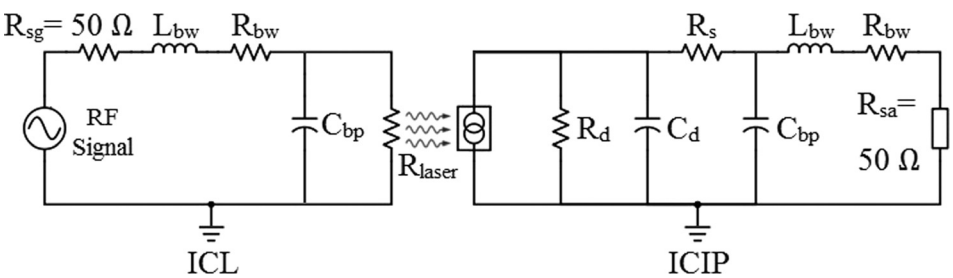

FIG. 5. High-frequency circuit model constructed for the interband cascade mid-IR system. R_{sg} and R_{sa} are the output or input resistance of the analog signal generator and the spectrum analyzer, respectively. All the other circuit parameters are denoted in Tables I and II.

TABLE I. Measured and simulated high-frequency circuit parameters for the IC laser working at $T = 293$ K.

Laser size ($\mu m \times \mu m$)	Laser resistance R_{laser} (Ω)	Bonding pad size ($\mu m \times \mu m$)	Bonding pad capacitance C_{bp} (pF)	Bonding wire inductance L_{bw} (nH)	Bonding wire resistance R_{bw} (Ω)	ICL simulated bandwidth (MHz)
20×2000	4.9	300×2000	77.4	3.4	0.06	757

TABLE II. Summary of the measured and simulated high-frequency circuit parameters for two different-sized ICIPs. The ICIP capacitance (C_d) was deduced from a fit to the measurement data.

Detector size (μm^2)	Device resistance R_d (kΩ)	Device capacitance C_d (pF)	Series resistance R_s (Ω)	Bonding pad size ($\mu m \times \mu m$)	Bonding pad capacitance C_{bp} (pF)	Bonding wire inductance L_{bw} (nH)	Bonding wire resistance R_{bw} (Ω)	Simulated ICIP bandwidth (MHz)	Simulated system bandwidth (MHz)	Measured system bandwidth (MHz)
20×20	35.1	1.04	101	100×100	1.1	11.1	0.44	1293	847	848
30×30	19.3	2.83	73	100×100	1.1	11.1	0.44	604	430	431

with the impedance matching circuits. It is worth noting that the frequency response of the single-stage ICIPs with thick absorbers was also investigated experimentally. These single-stage ICIPs with thick absorbers had bandwidths more than an order of magnitude narrower than the three-stage ICIP with thin individual absorbers, which validates the advantage of the multiple discrete absorber architecture.

In summary, the high-frequency operation ($f_{3\text{-}dB} > 800$ MHz) of an interband cascade system which is composed of an IC laser and an uncooled three-stage ICIP has been demonstrated at room temperature. This initial study shows that ICIPs (at zero-bias) can achieve gigahertz bandwidth with detectivities larger than 10^9 cm $Hz^{1/2}$/W at room temperature, suggesting great potential and the feasibility of compact systems for relevant applications. Nevertheless, many aspects such as carrier dynamics and transport mechanisms remain unexplored in interband cascade structures. Further research on the device physics, growth, and fabrication is desirable to provide more perspectives on the ultimate performance of interband cascade systems.

This work was supported in part by AFOSR under Award No. FA9550-15-1-0067.

[1]R. Q. Yang, Superlattices Microstruct. **17**, 77 (1995).
[2]J. V. Li, R. Q. Yang, C. J. Hill, and S. L. Chuang, Appl. Phys. Lett. **86**, 101102 (2005).
[3]R. Q. Yang, Z. Tian, J. F. Klem, T. D. Mishima, M. B. Santos, and M. B. Johnson, Appl. Phys. Lett. **96**, 063504 (2010).
[4]I. Vurgaftman, R. Weih, M. Kamp, J. R. Meyer, C. L. Canedy, C. S. Kim, M. Kim, W. W. Bewley, C. D. Merritt, J. Abell, and S. Höfling, J. Phys. D: Appl. Phys. **48**, 123001 (2015).
[5]A. Soibel, M. W. Wright, W. H. Farr, S. A. Keo, C. J. Hill, R. Q. Yang, and H. C. Liu, Electron. Lett. **45**, 264 (2009).
[6]A. Soibel, M. W. Wright, W. H. Farr, S. A. Keo, C. J. Hill, R. Q. Yang, and H. C. Liu, IEEE Photonics Technol. Lett. **22**, 121 (2010).
[7]D. Sawyer and R. Rediker, Proc. IRE **46**, 1122 (1958).
[8]R. Q. Yang, Z. Tian, Z. Cai, J. F. Klem, M. B. Johnson, and H. C. Liu, J. Appl. Phys. **107**, 054514 (2010).
[9]R. T. Hinkey and R. Q. Yang, J. Appl. Phys. **114**, 104506 (2013).
[10]Z. Tian, R. T. Hinkey, R. Q. Yang, D. Lubyshev, Y. Qiu, J. M. Fastenau, A. W. K. Liu, and M. B. Johnson, J. Appl. Phys. **111**, 024510 (2012).
[11]N. Gautam, S. Myers, A. V. Barve, B. Klein, E. P. Smith, D. R. Rhiger, L. R. Dawson, and S. Krishna, Appl. Phys. Lett. **101**, 021106 (2012).
[12]H. Lotfi, L. Lei, L. Li, R. Q. Yang, J. C. Keay, M. B. Johnson, Y. Qiu, D. Lubyshev, J. M. Fastenau, and A. W. K. Liu, Opt. Eng. **54**, 063103 (2015).
[13]H. Lotfi, L. Li, L. Lei, R. Q. Yang, J. F. Klem, and M. B. Johnson, J. Appl. Phys. **119**, 023105 (2016).
[14]W. Pusz, A. Kowalewski, P. Martyniuk, W. Gawron, E. Plis, S. Krishna, and A. Rogalski, Opt. Eng. **53**, 043107 (2014).
[15]Z. Tian, S. E. Godoy, H. S. Kim, T. Schuler-Sandy, J. A. Montoya, and S. Krishna, Appl. Phys. Lett. **105**, 051109 (2014).
[16]D. Hofstetter, M. Graf, T. Aellen, J. Faist, L. Hvozdara, and S. Blaser, Appl. Phys. Lett. **89**, 061119 (2006).
[17]A. Vardi, N. Kheirodin, L. Nevou, H. Machhadani, L. Vivien, P. Crozat, M. Tchernycheva, R. Colombelli, F. H. Julien, F. Guillot, C. Bougerol, E. Monroy, S. Schacham, and G. Bahir, Appl. Phys. Lett. **93**, 193509 (2008).
[18]D. Hofstetter, F. R. Giorgetta, E. Baumann, Q. Yang, C. Manz, and K. Köhler, Appl. Phys. B: Lasers Opt. **100**, 313 (2010).
[19]P. Reininger, T. Zederbauer, B. Schwarz, H. Detz, D. MacFarland, A. M. Andrews, W. Schrenk, and G. Strasser, Appl. Phys. Lett. **107**, 081107 (2015).
[20]B. Schwarz, D. Ristanic, P. Reininger, T. Zederbauer, D. MacFarland, H. Detz, A. M. Andrews, W. Schrenk, and G. Strasser, Appl. Phys. Lett. **107**, 071104 (2015).
[21]Y. Jiang, L. Li, R. Q. Yang, J. A. Gupta, G. C. Aers, E. Dupont, J. M. Baribeau, X. Wu, and M. B. Johnson, Appl. Phys. Lett. **106**, 041117 (2015).